Theory and applications of surface micro-kinetics in the rational design of catalysts using density functional theory calculations

Mao, Y., Wang, H., & Hu, P. (2017). Theory and applications of surface micro-kinetics in the rational design of catalysts using density functional theory calculations. *Wiley Interdisciplinary Reviews: Computational Molecular Science*, *7*(6), [e1321]. https://doi.org/10.1002/wcms.1321

Published in:
Wiley Interdisciplinary Reviews: Computational Molecular Science

Document Version:
Peer reviewed version

Queen's University Belfast - Research Portal:
Link to publication record in Queen's University Belfast Research Portal

Theory and applications of surface micro-kinetics in the rational design of catalysts using DFT calculations

Yu Mao[1,2], Hai-Feng Wang[1]*, and P. Hu[1,2]*

[1] *Key Laboratory for Advanced Materials, Research Institute of Industrial Catalysis and Centre for Computational Chemistry, East China University of Science and Technology, 130 Meilong Road, Shanghai, P. R. China, 200237.*

[2] *School of Chemistry and Chemical Engineering, The Queen's University of Belfast, Belfast, BT9 5AG, UK.*

Abstract

Rational design of catalysts has long been an important and challenging goal in heterogeneous catalysis. To achieve this target, density functional theory (DFT) calculations and micro-kinetics are two of the cornerstones. The DFT calculations make it possible to obtain microscopic properties of catalytic systems by computational simulations, and the micro-kinetic modeling of surface reactions provides a tool to link quantum-chemical data with macroscopic behaviors of the systems. In this review, we focus on the basic concepts and latest theoretical progresses of strategies for the catalysts design, including Brønsted−Evans−Polanyi (BEP) relation, the volcano curve, and the activity window. Among the progresses, the theory of chemical potential kinetics in heterogeneous catalysis and its implications on catalysts design, which was developed by our group, are described in detail with extensive derivations. Furthermore, the applications of this method on screening low-cost counter electrodes for dye-sensitized solar cells are presented with experimental evidences.

Introductory remarks

Heterogeneous catalysis is of paramount importance in a wide range of the chemical, biological, and energy industries,[1-4] such as CO oxidation,[5-7] steam reforming,[8-10] NO_X reduction,[11-13] and ammonia synthesis.[14-16] Rational design of efficient heterogeneous catalysts by quantum-chemical calculations, therefore, is currently an exciting and challenging target for researchers; however, traditional trial-and-error methods for producing new catalysts consume great efforts and time, which is inadequate to meet the demand of rapidly developing catalytic community.[17-22] The computational design approach, on the contrary, possesses great advantages and attracted much attentions in recent years. Firstly, computational simulations require only electricity and computers, which is considerably more economic and sustainable than synthesizing and testing candidate catalysts experimentally. Secondly, the traditional methods are limited by the experimental techniques; it is very difficult to manipulate the structure of catalysts at the atomic level. In the computational methods, on the other hand, the microscopic properties and composition of a certain material can be altered and sampled throughout whole possible candidates, which provides a broader and more diversified screening database. Thirdly and perhaps the most importantly, the performance of quantum-chemical calculations may improve significantly in the future with the rapidly developing information technology. In terms of hardware, the computational capacity has been increasing continually in the past decades, which doubles approximately every two years (Moore's law). In terms of software, more and more advanced computational packages and techniques would appear in coming years. For instance, the density functional theory (DFT) calculations were found to be

more accurate and affordable with random phase approximation,[23, 24] which may allow DFT calculations to be applied in larger systems. More examples can be found in Box 1.

Box 1. Advances and latest computational techniques for the rational design of catalysts

(a) Nørskov et al.[16] firstly showed that the rate of ammonia synthesis over a nanoparticle ruthenium catalyst can be calculated directly by DFT with a factor 3 to 20 of the experimental rate. They later introduced a general method for estimating the uncertainty in calculated properties of the material.[14, 25] (b) Martínez et al.[26] reported the application of the *ab initio* nanoreactor on discovering new pathways for glycine synthesis from primitive compounds existing on the early Earth, known as Urey–Miller experiment.[27] Graphics processing unit (GPU) architectures allow a big acceleration on the time-consuming first-principles molecular dynamics simulations.[28, 29] (c) Medford et al.[30] developed CatMAP, a code for descriptor-based micro-kinetic mapping of catalytic trends, which provides a useful tool for converting quantum-chemical properties of elementary reactions into macroscopic behavior of catalysts.[31] (d) Wang et al.[32] explored the possibility of designing catalysts beyond the traditional volcano curve.[33] They showed that with multi-phase catalysts, traditional constraints of the reaction rate would be broken, which provides a new idea for designing catalysts with high efficiency. The concepts of micro-kinetics and the volcano curve will be discussed in detail in the following sections. (Figure a-d are reprinted from ref.[16, 26, 30, 32] with permission from the American Association for the Advancement of Science, Nature Publishing Group, Springer, and the Royal Society of Chemistry, respectively)

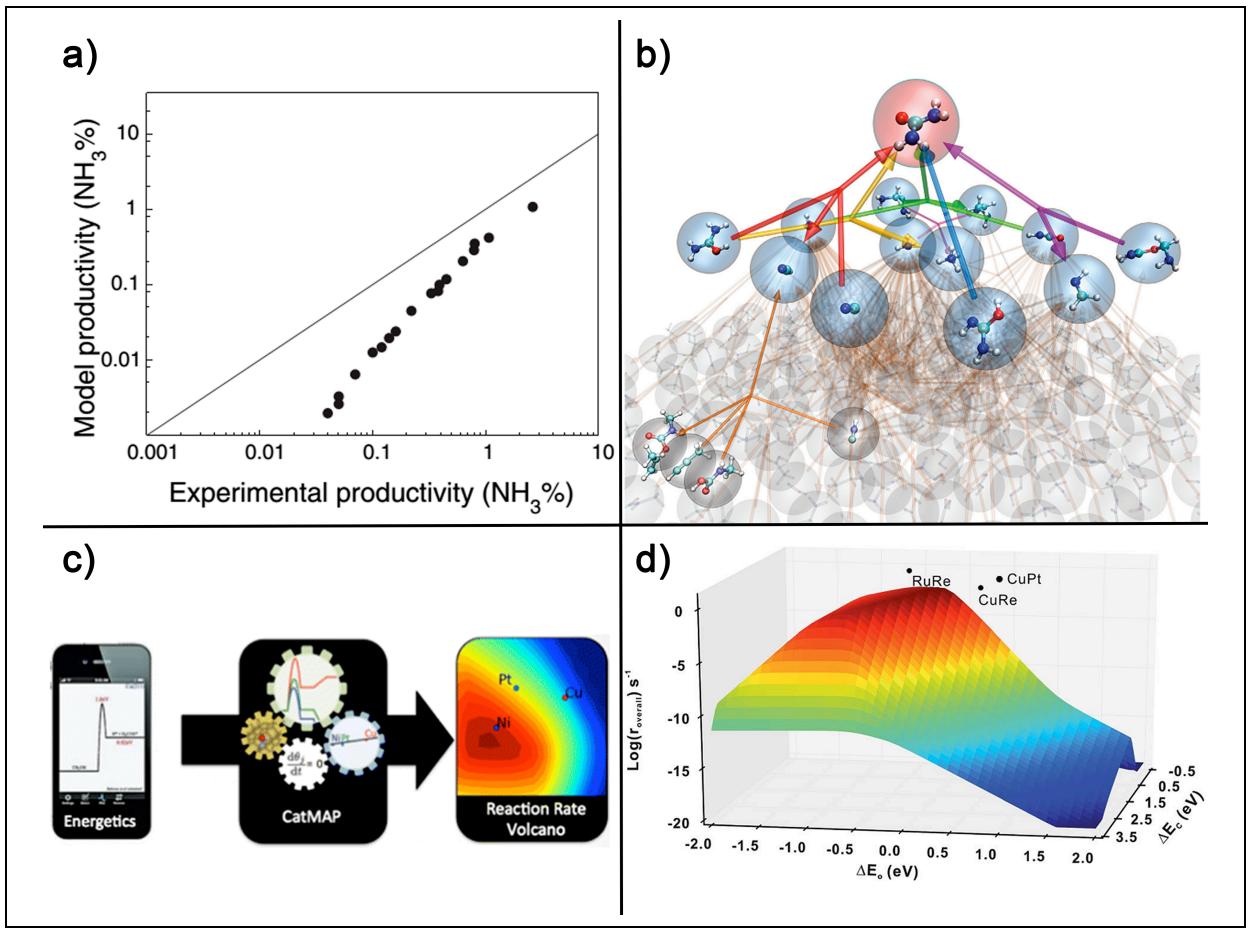

In this review, we firstly review the current understandings and useful relationships in heterogeneous catalysis, which is crucial for the rational design of catalysts. Then, different schemes of catalyst screening are introduced with contrast and comparison. After that, the paper is focused on the development and implications of the theory of chemical potential kinetics in heterogeneous catalysis. A detailed mathematical derivation is illustrated with comprehensive analysis on its implications towards the optimal adsorption energy window. In addition, the applications of this method on screening efficient counter electrode (CE) materials for dye-sensitized solar cells (DSSC) are discussed in the last part of the paper, which confirms its validity and reliability by experiments.

General understandings and relationships in the rational design of catalysts

Computational catalyst design requires deep understandings of the reactivity and selectivity in heterogeneous catalysis. In the past two decades, with the popularization of DFT calculations[34-36] and micro-kinetics,[37-39] many reaction mechanisms and general relations on heterogeneous catalysis were unveiled. For example, the hydrogen oxidation reaction ($2H_2 + O_2 \rightarrow 2H_2O$), which has been studied since the early 19th century, is the first identified surface catalytic reactions in the history.[40-42] The reaction would be considerably facilitated on contact with Pt surfaces at room or even lower temperature. Despite its apparent simplicity, however, not until the application of DFT calculations on Pt surfaces was the mechanism of hydrogen oxidation reactions clearly figured out. In our previous study,[42] DFT calculations on the elementary steps of this reaction revealed that H_2O formation from chemisorbed O and H atoms on Pt(111) surface is a highly activated process. OH will be produced from the chemisorbed O and H with a barrier ~1 eV; once formed, OH groups are easily hydrogenated to H_2O (barrier ~0.2 eV). Furthermore, H_2O was shown to act as autocatalysts in this process, since the disproportionation reaction of H_2O and O with 2:1 stoichiometry is more preferred than that with 1:1 stoichiometry both thermodynamically and kinetically. These theoretical findings play an important role in understanding its intrinsic mechanism.

More importantly, a clear picture of reaction mechanism is one of the prerequisites for the rational design of catalysts; general relations and activity trends on heterogeneous catalysis are also necessary in order to screen a wide range of possible candidates in a high-throughput way. Regarding the activity trends of catalysts, the volcano curve is arguably the most important

finding, which can be explained by Sabatier's principle.[43, 44] Qualitatively, an excellent catalyst should have a moderate binding ability, neither too strong nor too weak, and thus along the adsorption energy axis, the catalytic activity would rise initially and then fall, leading to a volcano-shape curve (Fig. 1).

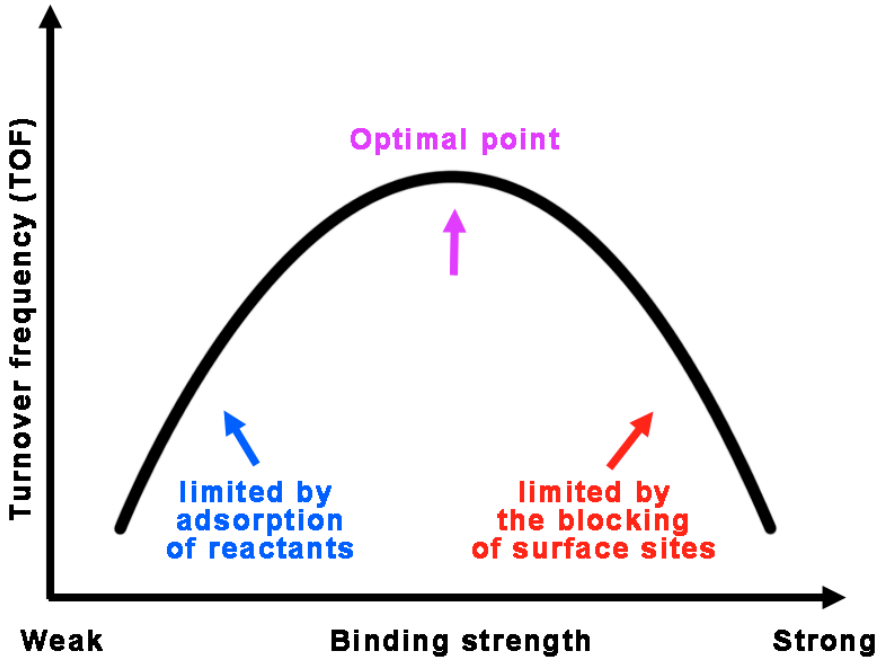

Figure 1. Schematic representation of the Sabatier's principle and the volcano curve.

Quantitatively, it is the identification of the Brønsted-Evans-Polanyi (BEP)[33, 45-48] relation and scaling relation[49, 50] that provide a foundation to unveil the origin of the volcano curve. Figure 2 shows a typical heterogeneous catalytic reaction: the reactant (R) adsorbs on a surface as the intermediate (I), followed by surface reaction and desorption of the product (P). For the adsorption process, the barrier of dissociative adsorption (E_R^{dis} in Fig. 2) are correlated to the adsorption energy ($E_{ad,R}$ in Fig. 2). This correlation has been well established for many reactions, such as C–C, C–O, C–N, N–O, and O–O.[51] For example, the energy barrier of N_2 adsorption in

ammonia synthesis is related to the stability of N. The less stable the N is, the higher the energy barrier is for N_2 dissociative adsorption. Similar relation also applies to the desorption barrier (E_P^{dis} in Fig. 2) and the adsorption energy of the product ($E_{ad,P}$ in Fig. 2).

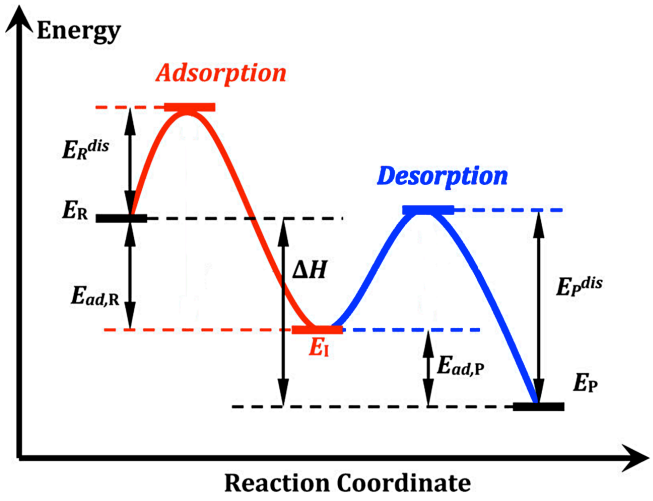

Figure 2. Schematic profile of a two-step model taking into consideration the dissociative adsorption of reactants and associative desorption of products on a heterogeneous catalyst surface. ΔH is the enthalpy change of the overall reaction. E_R and E_P are total energies of the gaseous reactants and products, respectively. $E_{ad,R}$ and $E_{ad,P}$ are the adsorption energies of the reactants and the products, respectively. E_R^{dis} and E_P^{dis} are the barriers for the adsorption and desorption processes. E_I is the energy of the intermediate state. Adapted from ref.[52] with permission from American Chemical Society.

Similarly, the scaling relation indicates that there are linear relationships between adsorption energies of similar adsorbates, and for a complicated system, the energies of all intermediates can usually be related to one or two key intermediates.[50, 53] Therefore, with the BEP and scaling relations, the reaction rate can finally be expressed as a function of the adsorption energy of one or two key intermediates by solving the micro-kinetics of the catalytic system.[30, 54] As shown in Figure 1, when the adsorption strength is weak, the whole reaction is limited by the activation of the reactant; if the binding is strong, the desorption of the product

would be limited. Therefore, the peak of the curve would locate in a moderate bonding strength. With a full analytical derivation of the micro-kinetics on a two-step catalytic model, we showed that plotting this function for a heterogeneous catalytic reaction will always lead to a volcano curve, which can be deemed as an essential property, and it is the poison of the surface by intermediates rather than the desorption barrier that limited the desorption process.[54]

In the volcano curve, the adsorption energy of key intermediates can be used as descriptors for predicting the performance of candidate catalysts. By comparing DFT chemisorption energies with experimental ones, Nørskov et al.[46, 55] firstly found that the optimal adsorption energy lies in a "chemical window" between -2 to -1 eV in most cases. They then developed a descriptor-based linear-scaling approach to screen catalysts, which can be briefly summarized as the following steps: (i) determine the reaction mechanism of the target system; (ii) develop a micro-kinetic model according to the mechanism; (iii) assuming similar mechanism on all candidate materials, develop BEP and scaling reaction, which correlate energies of intermediates and transition states with one or two key intermediates (descriptors); (iv) plot the volcano curve/surface by solving the micro-kinetics; and (v) choose a candidate material and calculate its values of descriptors. Then the performance of this candidate can be estimated by comparing the descriptor values to the volcano curve. This method is quite robust and has been successfully used in many catalytic systems to find new catalysts.[22, 56-59] Campbell et al.[21] recently proposed a new screening method based on the concept of the degree of rate control (DRC). DRC is a good indicator for quantifying to what extent the free energy of each species can affect the overall reaction rate.[60, 61] A species with a larger DRC influences the whole

reaction more significantly. The implementation of DRC method is similar to the approach of Nørskov et al., except that DRC method uses the energies of the few species with the highest DRCs for the reference catalyst as descriptors to estimate the rates on related materials and predict the best one. This method can avoid solving micro-kinetics, which is usually the most difficult step in the catalyst design, provided that the DRCs are already known approximately. They suggested that the results are slightly more accurate than that of Nørskov et al. when candidate metals are similar to the reference metal. However, this method is not as robust as the former one when there are large changes in material types.

One disadvantage of the above descriptor-based methods is that there are too many possible materials on the desired descriptor range, including alloys, oxides, and supported metals. Creating such databases demands considerable time and computational resources. Being different from the descriptor-based methods, Sautet et al.[62, 63] introduced "coordination-activity plots" that outline the geometric structure of optimal active sites. They showed that there is correlation between the adsorption energy and the generalized coordination numbers, a number related with first and second nearest neighbor atoms of the adsorption site. Thus, the performance of the catalyst can be finally related with this coordination numbers. For oxygen reduction reaction (ORR) on Pt(111), they found that sites with same number of first-nearest neighbors but increased number of second-nearest neighbors are more active and subsequently prepared highly active Pt(111) active sites without alloying by three affordable experimental methods. Wang and Hu[17] proposed a general optimization framework for catalyst design: With DFT calculations and micro-kinetics, the reaction rate can be expressed as a function of the

energies of surface species, and the energies of surface species as a function of catalyst structure. Therefore, the reaction rate is finally a function of the catalyst structure. One can subsequently apply some optimization method (*e.g.* gradient descent algorithm) on this function to find better catalyst structures for a specific catalytic reaction.

Chemical potentials and optimal adsorption energy window

The Sabatier principle and volcano curve mentioned above serve as the cornerstone in the rational design of catalysts, which enable us to predict the trend of activity on catalysts over the periodic table qualitatively. However, more intrinsic and quantitative understandings toward their origins and the optimal adsorption energy window was inadequate. To quantitatively understand the optimal adsorption energy window, we introduced the concept of chemical potential in heterogeneous catalysis.[64] We here revisit the derivation of the chemical potential in the following equations. Starting from the chemical potential of the ideal gas, its chemical potential can be expressed as function of partial pressure p at a given temperature T:

$$\mu(T,p) = \mu^o(T,p^o) + RT\ln\frac{p}{p^o} \tag{1}$$

where $\mu^o(T, p^o)$ is the chemical potential at the standard pressure (p^o = 1 bar). It should be noted that the chemical potential is equal to molar Gibbs free energy in the ideal gas model ($\mu = G_m = G/N$). Choosing the temperature of 0 K as reference, equation (1) can be expanded as:

$$\begin{aligned}\mu(T,p) &= \mu^o(0K,p^o) + [H_m(T,p^o) - H_m(0K,p^o)] - TS_m(T,p^o) + RT\ln\frac{p}{p^o} \\ &= \mu^o(0K,p^o) + \Delta\mu(T,p^o) + RT\ln\frac{p}{p^o}\end{aligned} \tag{2}$$

where H_m, S_m, and G_m represent the molar enthalpy, entropy, and Gibbs free energy, respectively;

and the relations that $G_m = H_m - TS_m$ and $S_m(0\ K) = 0$ are used. $\Delta\mu(T, p^o)$ can be regarded as the thermal correction term of the chemical potential under T K. The difference of enthalpy at different temperature is usually small; therefore, $\Delta\mu(T, p^o)$ is dominated by the entropy term $-TS_m(T, p^o)$. In the following, we will drop the labels of pressure for simplicity.

For the chemical potentials of adsorbates on a surface, the coverage-dependent μ can be derived according to the Langmuir adsorption paradigm.[31, 65, 66] Given that (i) the surface contains M distinguishable sites; (ii) N_i and q_i correspond to the number and partition function of surface species i (i = 0 in the case of free site); and (iii) one species occupies one site, we will have:

$$M = \sum_{i\geq 0} N_i \tag{3}$$

The partition function of free sites (q_0) can be considered to be unity which consists only of high-frequency vibrational modes of substrate atoms. For surface species, q_i are constituted merely by vibrational modes, because their translation and rotation are rather limited.[31, 65, 66] Thus, the total partition function of this system can be expressed as:

$$Q(T, M, N_i) = M! \prod_{i\geq 0} \frac{q_i^{N_i}}{N_i!} = \frac{M!}{N_0!} \prod_{i\geq 1} \frac{q_i^{N_i}}{N_i!} \tag{4}$$

Taking logarithm and using Stirling's approximation, we obtain:

$$\begin{aligned} \ln Q &= M \ln M - M + \sum_{i\geq 0} N_i \ln q_i - \sum_{i\geq 0} N_i \ln N_i + \sum_{i\geq 0} N_i \\ &= M \ln M + \sum_{i\geq 1} (N_i \ln q_i - N_i \ln N_i) - N_0 \ln N_0 \end{aligned} \tag{5}$$

For surface species i, the chemical potential is:

$$\mu_i(T, N_i) = -RT \left(\frac{\partial \ln Q}{\partial N_i}\right)_{T, N_j} \quad j \neq 0,\ i \neq j \tag{6}$$

Substituting equation (3) and (5) into equation (6), it can be written as:

$$\mu_i(T, N_i) = -RT(\ln q_i - \ln N_i + \ln N_0) = -RT \ln q_i + RT \ln \frac{N_i}{N_0} \tag{7}$$

Considering the surface coverage θ, equation (7) can be rewritten as:

$$\mu_i(T, N_i) = -RT \ln q_i + RT \ln \frac{\theta_i}{\theta_0} \tag{8}$$

where θ_0 and θ_i stand for the surface coverages of free sites and species i, respectively. Defining $-RT\ln q_i$ as $\mu^o(T)$, the standard chemical potential of surface species i, and using θ_* to represent θ_0, we obtain:

$$\mu_i(T, \theta_i) = \mu_i^o(T) + RT \ln \frac{\theta_i}{\theta_*} \tag{9}$$

The presence of θ_* in the equation reflects that in the Langmuir adsorption model surface species need to be accommodated at certain adsorption sites, whereas in the gas or liquid phases there are no such counterparts. Similar to our treatment with gas phase molecules in equation (2), equation (9) can be further expanded as:

$$\begin{aligned} \mu_i(T, \theta_i) &= \mu_i^o(0K) + [H_{m,i}(T) - H_{m,i}(0K)] - TS_{m,i}(T) + RT \ln \frac{\theta_i}{\theta_*} \\ &= \mu_i^o(0K) + \Delta\mu_i(T) + RT \ln \frac{\theta_i}{\theta_*} \end{aligned} \tag{10}$$

Since the entropy contribution equals to zero at 0 K, term $\mu^o(0\ K)$ is essentially equivalent to the total energy (E^{tot}) of a molecule or system with corrected zero point energy (ZEP), which can be directly obtained from DFT calculations. The thermal correction term $\Delta\mu(T)$ in equation (10) is rather different from that in equation (2) which contains a large entropy term $TS_m(T)$; actually, the entropies of simple adsorbed species are usually very small and often ignored in

micro-kinetic treatment. Therefore, referring μ_i^o to $\mu_i^o(T)$ and E_i^{tot} to $\mu_i^o(0\mathrm{K})$, we obtain the expression of chemical potential for surface species:

$$\mu_i = \mu_i^o + RT\ln\frac{\theta_i}{\theta_*} = E_i^{tot} + RT\ln\frac{\theta_i}{\theta_*} \tag{11}$$

Similarly, equation (2) for gas phase molecules can be rewritten as:

$$\mu = \mu^o + RT\ln\frac{p}{p^o} = E^{tot} - TS + RT\ln\frac{p}{p^o} \tag{12}$$

With this chemical potential formulation, many micro-kinetic expressions, including rate equations, reversibility, and coverage can be reformulated in rather simplified forms. To demonstrate this, we will employ a two-step catalytic model which comprises both adsorption and desorption processes:

$$\mathrm{R(g)} + * \xrightarrow{adsorption} \mathrm{I}* \xrightarrow{desorption} \mathrm{P(g)} + * \tag{13}$$

It captures the key characteristics of many heterogeneous catalytic reactions and has been used in our previous work.[19, 52, 54, 64, 67-69] Under the traditional micro-kinetic framework, the rate equations of reaction (13) can be written as:[31, 39, 70, 71]

$$r_{ads} = \frac{k_B T}{h} e^{\frac{-\Delta G_R^{\neq,o}}{RT}} \frac{p_R}{p^o}\theta_*(1 - z_{ads}); \quad r_{des} = \frac{k_B T}{h} e^{\frac{-\Delta G_P^{\neq,o}}{RT}} \theta_I(1 - z_{des}) \tag{14}$$

$$z_{ads} = \frac{\theta_I}{K_{eq1}\theta_* \, p_R / p^o}; \quad z_{des} = \frac{\theta_* \, p_R / p^o}{K_{eq2}\theta_I} \tag{15}$$

where z_{ads} (z_{des}) stands for the reversibility of the adsorption (desorption) process;[71] $\Delta G_R^{\neq,o}$ ($\Delta G_P^{\neq,o}$) is the standard Gibbs free energy difference between the transition state and the initial state of the adsorption (desorption) process; K_{eq1} (K_{eq2}) represents equilibrium constant of the adsorption (desorption). Based on the theory of chemical potential kinetics, specifically,

equation (11) and (12), equation (14) and (15) can be reformulated as:

$$r_{ads} = \frac{k_B T}{h} e^{\frac{\mu_R - \mu_R^{\neq,o}}{RT}} \theta_* (1 - z_{ads}); \quad r_{des} = \frac{k_B T}{h} e^{\frac{\mu_R - \mu_P^{\neq,o}}{RT}} \theta_* z_{ads} (1 - z_{des}) \tag{16}$$

$$z_{ads} = e^{\frac{\mu_I - \mu_R}{RT}}; \quad z_{des} = e^{\frac{\mu_P - \mu_I}{RT}} \tag{17}$$

where $\mu_R^{\neq,o}$ ($\mu_P^{\neq,o}$) is the standard chemical potential of the transition states of the adsorption (desorption) processes; μ_R (μ_P) stands for the chemical potential of the reactant (product). It should be noted that in the derivation the transition states are regarded as surface adsorbates; therefore, their entropy contributions are ignored.

According to the BEP relation we mentioned before, $\mu_R^{\neq,o}$ and $\mu_P^{\neq,o}$ are lineally related to μ_I^o, which is a intrinsic property and independent of reaction conditions. Therefore, with the constraint of surface conservation $\theta_* + \theta_I = 1$ and the steady state approximation $r = r_{ads} = r_{des}$,[31, 39, 70], the overall reaction rate r (turnover frequency TOF) can be expressed as a function with a single variable μ_I^o (equivalent to the adsorption energy of intermediate *I*). Notably, plotting μ_I^o against r of this function would lead to a typical volcano curve.[33, 54]

Compared to the traditional kinetic equations for catalytic reactions, what can we learn from the kinetics of chemical potentials? Typically, to obtain a good reaction rate, the chemical potentials of the reactants, intermediates, and products should decrease step by step (Fig. 3):[64]

$$\mu_R > \mu_I > \mu_P \tag{18}$$

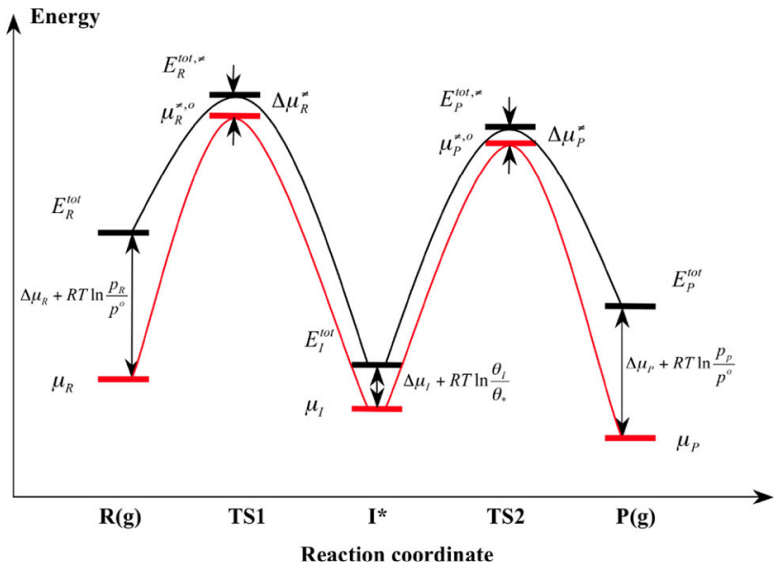

Figure 3. Energy diagram of a model for heterogeneous catalytic reactions. The black curve stands for the profile of total energies calculated from DFT, and the red curve represents the profile of chemical potentials. TS1 and TS2 are the transition states (TSs) of adsorption and desorption, respectively. E^{tot} is the total energy, and μ is the chemical potential (subscript R, I and P refer to reactant, intermediate, and product, respectively). $E_R^{tot,\neq}$ and $\mu_R^{\neq,o}$ are the total energy and standard chemical potential of the TS of adsorption, respectively; $E_P^{tot,\neq}$ and $\mu_P^{\neq,o}$ have the same meanings for the TS of desorption. The correction of the chemical potential because of the temperature effect is given by $\Delta\mu$. The thermal corrections for gaseous molecules ($\Delta\mu_R$ and $\Delta\mu_P$) are quite large because of large entropy effects, whereas the corrections for surface species are much smaller. $RT\ln(\theta_i/\theta_*)$ is the coverage-dependent term in the expression of the chemical potential of surface species, and likewise $RT\ln(p/p^o)$ is the pressure-dependent term for gaseous molecules. Unlike intermediate state, the standard chemical potentials for the TSs appear in the profile of chemical potentials. Adapted from ref.[64] with permission from Wiley-VCH.

Applying equation (11), equation (18) can be expanded as:

$$\mu_R + RT\ln\frac{\theta_I}{\theta_*} > \mu_I^o + RT\ln\frac{\theta_I}{\theta_*} > \mu_P + RT\ln\frac{\theta_I}{\theta_*} \tag{19}$$

As proved in our original paper,[64] θ_* is usually in the range between 0.01 and 0.1 at the steady state for good catalysts. For example, θ_* is around 0.08 for hydrogenation of isobutene on Pt[71] and around 0.01 for ammonia synthesis on Fe and Ru surfaces.[47, 71] It is quite reasonable that θ_* for a good catalyst should not be too large or too small, either of which would hinder the

whole reaction. Therefore, the magnitude of the coverage-dependent $RT\ln(\theta_I/\theta_*)$ has to be a small term, typically about 0.1–0.2 eV at 500 K. Defining this term as ε and substitutes it in equation (19), we have:[64]

$$\mu_R+\varepsilon > \mu_I^o > \mu_P+\varepsilon \tag{20}$$

where the ε for μ_I^o is ignored.

Equation (20) is a fundamental equation for catalyst screening: a good catalyst should typically lie in the range between the chemical potential μ_R and μ_P as lower and upper bounds (blue zone in Fig. 4). For example, catalyst C in Figure 4 is likely to be active since it lies in the blue zone. Taking the coverage-dependent term ε into consideration, the region may be extended slightly as the red zone in Figure 4; therefore, D shall be also deemed as good catalyst. Catalyst A and B, which are outside of the red region, may exhibit much lower activities. According to this principle, the adsorption energy of N_2 of "good catalysts" in ammonia synthesis should be -1.7 ~ -0.8 eV, which agrees well with the chemical window found by Nørskov et al.[46, 55]

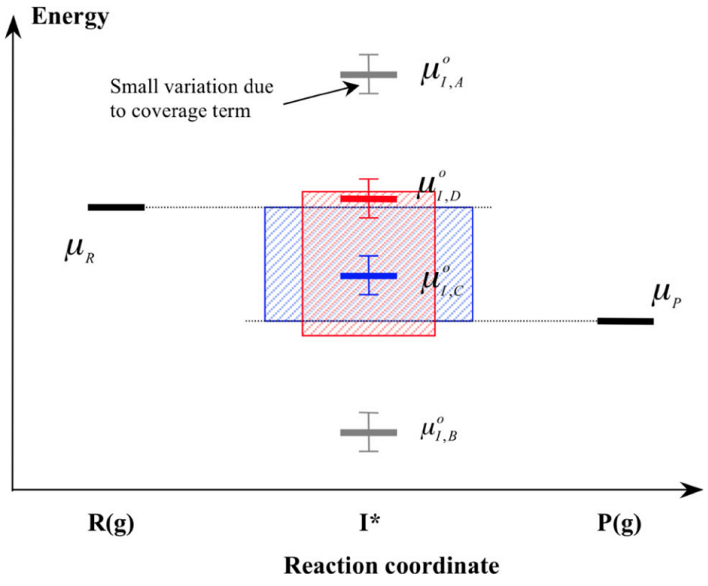

Figure 4. Searching for good catalysts by means of the involved chemical potentials. The chemical potentials of reactant and product (μ_R and μ_P) set the boundaries for the chemical potential of the surface intermediate (μ_I, blue zone). On good catalysts, this zone can only be slightly relaxed for the standard chemical potential of the surface intermediate (μ_I^o, red zone). Thus, surfaces of catalysts related to $\mu_{I,C}^o$ and $\mu_{I,D}^o$ are very likely to be good catalysts, whereas surfaces related to $\mu_{I,A}^o$ and $\mu_{I,B}^o$ cannot be good catalysts. Adapted from ref.[64] with permission from Wiley-VCH.

By carrying out detailed micro-kinetic analyses, Yang et al.[52] obtained a deeper understanding of equation (20). As shown in the left panel of Figure 5, for a two-step catalytic reaction (13) the activity trend would be the red line if the adsorption is the rate-determining step, while the blue line would represent the activity if the desorption is rate-determining. Interestingly, the values of $E_{ad,R,max1}$ and $E_{ad,R,max2}$, the maximum of the red and blue lines, can be determined analytically by solving partial differentials. It turns out that the value of $E_{ad,R,max1}$ and $E_{ad,R,max2}$ are very close to μ_P and μ_R, respectively, which unveils a clear physical picture for the chemical window: the optimal catalyst should lie above the maximum of adsorption-determining reaction and below the maximum of desorption-determining reaction (left panel, Fig.5); namely, neither adsorption nor desorption should dominate the whole reaction in order to have a good overall performance.

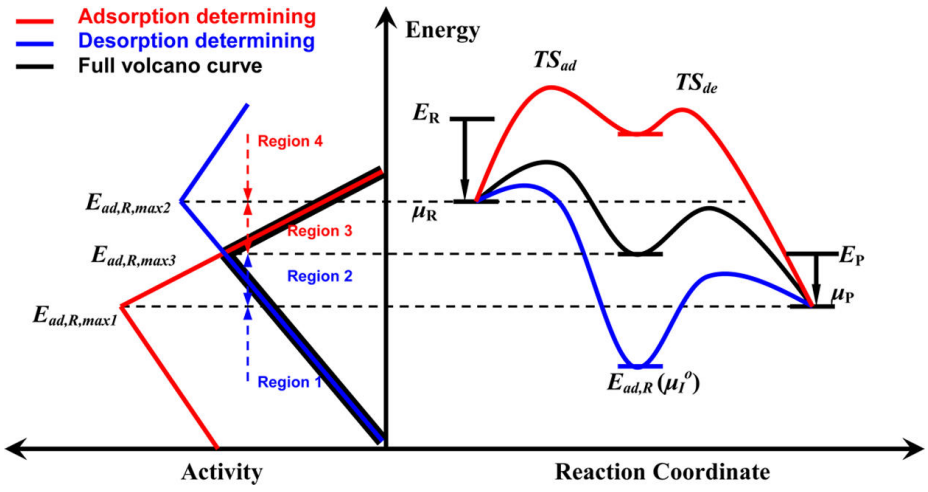

Figure 5. Schematic diagram of the volcano curves associated with reactions in which the adsorption (red) and desorption (blue) are rate determining, together with the real volcano curve (black) (left). The right side of the figure shows the energy profiles on three typical catalysts. μ_R and μ_P are the chemical potentials of the gaseous reactants and products, respectively. Reprinted from ref.[52] with permission from American Chemical Society.

Finally, it is worth mentioning that there are some similarities on the basic principles of this method and the descriptor-based linear-scaling approach we mentioned in the last section; both of them are targeting for a "window" of key intermediates. However, by considering the surface entropy and gas-phase pressure, which are lumped into the chemical potential term, our method, rooted on solid kinetic derivations, are more general and can be easily extended to photocatalysis and electrocatalysis. In addition, our method well explains the physical origin of the "window": it is resulted from a step-by-step decrease of the chemical potentials of the reactants, intermediates, and products.

Applications of optimal adsorption energy window in the design of counter electrode materials of dye-sensitized solar cells

The global demand for renewable energy is increasingly significant in past few decades. Among that, the solar energy is of great abundance and environmentally friendliness that attract much attention in recent years. Dye-sensitized solar cells (DSSC), invented by Grätzel et al,[72] are one of the solutions to make efficient and low-cost collection and conversion of the solar energy (Box 2). Traditionally, Pt is used as the counter electrode (CE) material in DSSC owing to its high activity and superb stability in the I^-/I_3^- electrolyte. Due to its high price, scientists are now actively searching for efficient alternative CE materials to replace Pt, including

polymers,[73, 74] transition metal sulphide/oxides,[75, 76] and carbon materials (e.g. graphene).[77, 78] Employing the chemical potential kinetic theory and optimal adsorption energy window mentioned above, we successfully identified the most active Pt facet[79] and predicted a range of novel CE materials for DSSC, including rust (α-Fe_2O_3),[19] RuO_2 Nanocrystals,[76] and NiS nanosheets,[75] which provide possible alternatives for the traditional Pt electrode. In addition, based on our screening criteria, we successfully converted indium oxide (In_2O_3), an inert CE material for DSSC, into a superior electrocatalyst by inserting nitrogen into In_2O_3 bulk structure.[80]

Box 2. Dye-sensitized solar cells (DSSC)

DSSC are promising and inexpensive alternatives to the traditional silicon based solar cells to convert solar energy.[81-84] The device has a sandwich structure that comprises a dye-sensitized mesoporous nanocrystalline semiconductor photoanode, a counter electrode (CE), and an electrolyte redox couple (e.g. I^-/I_3^-) as show in the illustration. The processes 1–7 in the figure represent: (1) electrons promotion to the excited state; (2) electron injection into the conduction band of semiconducting photoanode material; (3) electron transport and collection at the substrate; (4) reduction of the oxidized redox mediator; (5) reduction of the dye molecule by the redox mediator; (6,7) electrons recombination. (The figure reprinted from ref.[81] with permission from the Nature Publishing Group.)

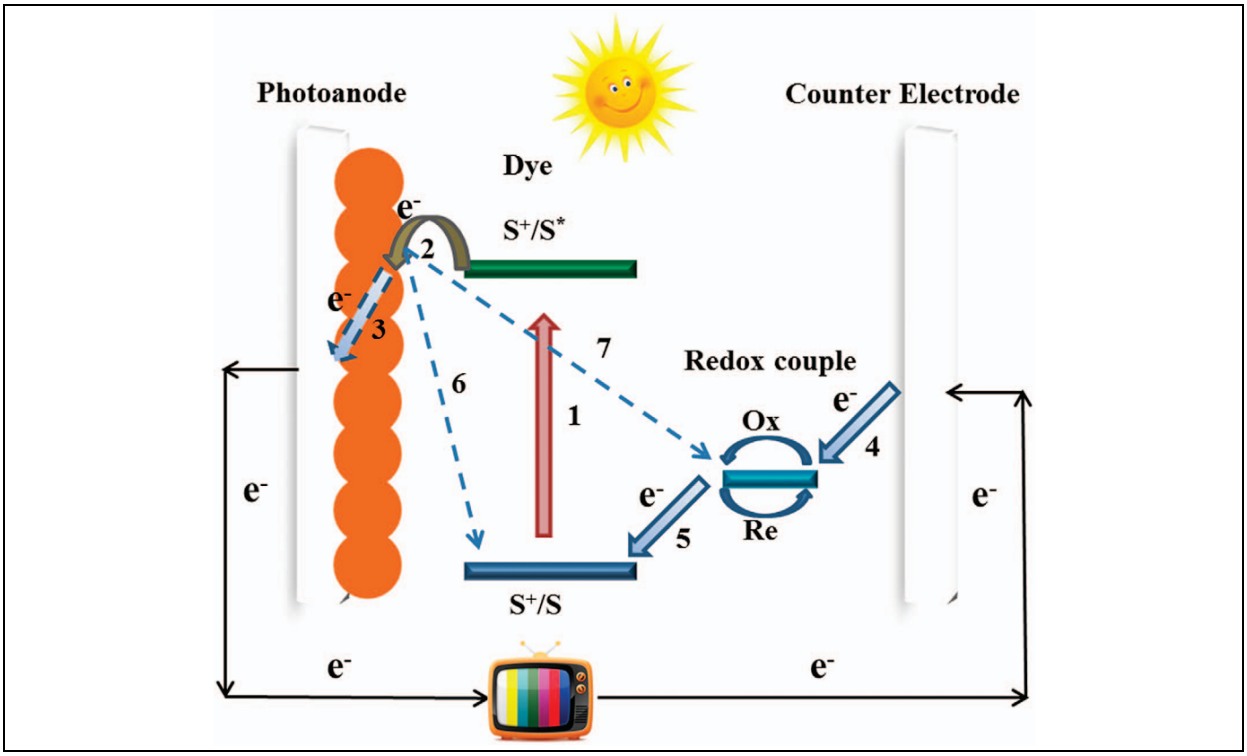

Let us start with the overall triiodide reduction reaction occurring on the CE:

$$I_3^-(sol) + 2e^- \rightarrow 3I^-(sol) \tag{21}$$

which includes three elementary steps:

$$I_3^-(sol) \rightarrow I_2(sol) + I^-(sol) \tag{22}$$

$$I_2(sol) + 2* \rightarrow 2I* \tag{23}$$

$$I* + e^- \rightarrow I^-(sol) \tag{24}$$

where sol indicates the acetonitrile (CH_3CN) solution and * stands for the free site on the electrode surface. Reaction (22) is usually fast and can be treated to be in equilibrium in solution,[85] and the subsequent iodine reduction reaction (IRR) (23) and (24), which occur at the liquid/solid interface, would therefore determine the overall activity. As shown in Figure 6, there are three states in IRR: $I_2 + 2e^-$, 2I*, and $2I^-$(sol). Among the steps, only the energy of 2I* can vary on different catalysts. According to equation (18), the chemical potential of 2I* on

good CE material should obey:

$$\mu_{I_2}(sol) + 2\mu_e \geq 2\mu_{I*} + 2\mu_e \geq 2\mu_{I^-}(sol) \tag{25}$$

where μ_{I2}, μ_e, μ_{I*}, μ_{I-} are the chemical potentials of I_2, electron, I*, and I^-, respectively. Applying equations (9) and (20) on equation (25) and expanding chemical potential into entropy and enthalpy terms, we can obtain:

$$\frac{1}{2}T\Delta S_{I_2} - \frac{1}{2}\Delta\mu_{I_2} - \varepsilon \leq \mu^o_{I*} \leq \frac{1}{2}T\Delta S_{I_2} + \frac{1}{2}\Delta G_0 - \frac{1}{2}\Delta\mu_{I_2} \tag{26}$$

where ε is the small term $RT\ln(\theta_{I*}/\theta_*)$, about 0.06 ~ 0.12 eV in this case;[19] $T\Delta S_{I2}$ is the entropy correction term in the gas phase at 298 K; $\Delta\mu_{I2}$ stands for the difference of chemical potential between I_2 in the gas phase and solvent; ΔG_o represents the Gibbs free energy change of half IRR:

$$\Delta G_o = \left(\mu_{I_2}(sol) + 2\mu_e\right) - 2\mu_{I^-}(sol) \tag{27}$$

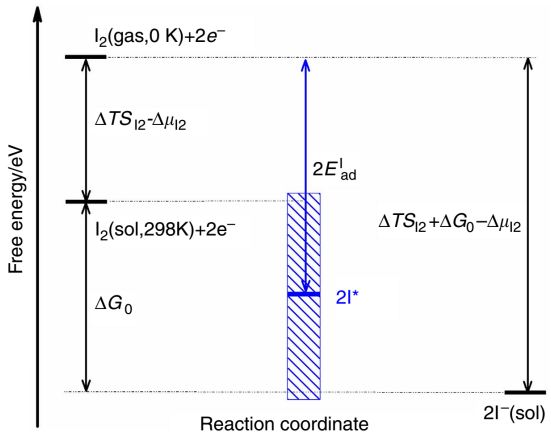

Figure 6. Demonstration of range estimation model for the suitable electrodes in terms of the adsorption energy of I atom. $T\Delta S_{I2}$ is the entropy correction term of I_2 in gas phase, $\Delta\mu_{I2}$ is chemical potential difference of I_2 molecule in between gas phase and CH_3CN solvent at 298K and ΔG_0 is the Gibbs free-energy change of half reaction $I_2(sol) + 2e^- \rightarrow 2I^-(sol)$. Reprinted from ref.[19] with permission from the Nature Publishing Group.

We designed a thermodynamic cycle combining the standard hydrogen electrode (SHE) to obtain the value of ΔG_o, which is very difficult to calculate directly.[19] Substituting all the

relevant values into equation (26), the adsorption energy window for good IRR catalysts was finally determined to be 0.33 to 1.20 eV (the region between two violet red dash line in Fig. 7). Based on this, the adsorption energies of I on a wide range of materials were calculated as shown in Figure 7, including the reported active materials (blue triangles), unreported materials (black squares), and materials we were interested in our research (red pentagons).

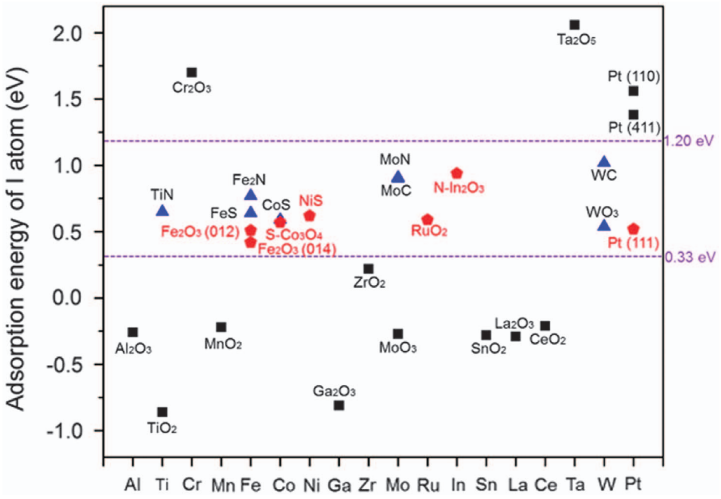

Figure 7. Calculated adsorption energy of I atom in the gas phase or in the CH_3CN solvent using DFT method. Blue triangles indicate the reported active materials; black squares represent the unreported materials, which were predicted to be less catalytically active; red pentagons stand for the materials tested in our research. For materials on which the adsorption of iodine atom is endothermic, solvent effects were not considered any more. Adapted from ref.[19, 81] with permission from the Nature Publishing Group.

Before introducing the applications of this chemical potential window, it is worth mentioning that we recently made a more systematic and comprehensive kinetic study on IRR to determine its optimal point on the active region (0.33 ~ 1.20 eV).[86] In Figure 8a, we uncovered two BEP relations for reactions (23) and (24). With these two relations, we solved the micro-kinetics of the IRR under different reaction conditions. According to the volcano curves shown in Figure 8b, the optimal adsorption energy of I is 0.43 eV.

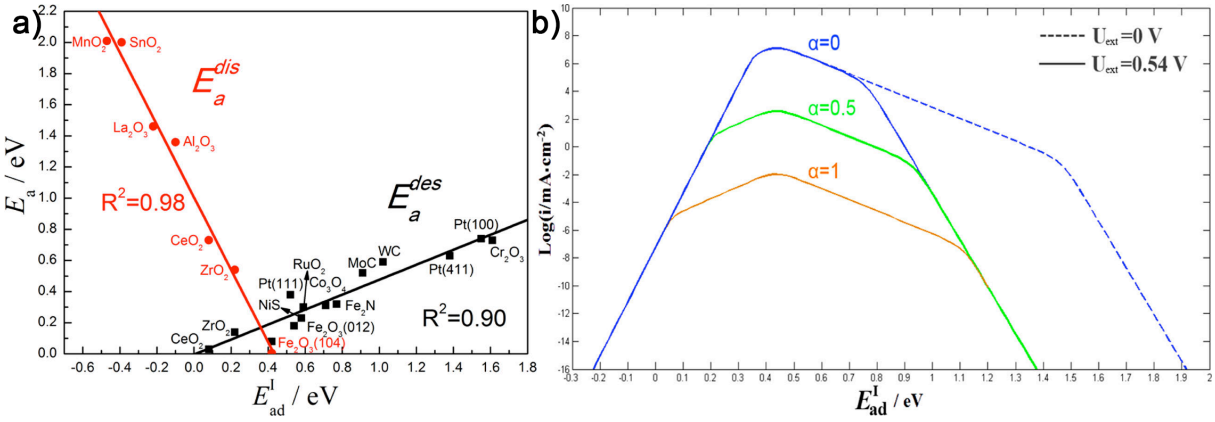

Figure 8. (a) Illustration of calculated E_a^{dis} of I_2 dissociation (red dots) and E_a^{des} for I* desorption (black squares) in a neutral system (U_{ext} = 0 V) as a function of E_{ad}^{I}. (b) Calculated volcano curves for IRR as a function of E_{ad}^{I} under different external voltage U_{ext} (dashed line, under open-circuit condition, U_{ext} = 0 V; solid line, 0.54 V), in which three different transfer coefficients for the I* desorption step are considered (blue, 0; green, 0.5; yellow, 1). Adapted from ref.[86] with permission from American Chemical Society.

It is clear from the discussions above that μ_{I*}^{o} of good CE materials for DSSC should lie between 0.33 and 1.20 eV, and the optimal point would be 0.43 eV. Based on this design guidance, we firstly investigated the facet-dependent catalytic behavior of three different Pt surface (100, 111, 411).[79] As shown in Figure 7, both Pt(100) (μ_{I*}^{o} = 1.56 eV) and Pt(411) (μ_{I*}^{o} = 1.38 eV) are outside of the "good catalyst region" whereas Pt(111) (μ_{I*}^{o} = 0.52 eV) is near the optimal point. The result revealed that Pt(111) is the most active Pt facet on catalysing IRR, which is near the peak of the volcano curve. Surprisingly, in our screening results in Figure 7, μ_{I*}^{o} of F_2O_3(012) and Fe_2O_3(104) are very close that on Pt(111), which made it reasonable to expect a high IRR activity of Fe_2O_3, one of the most low-cost and abundant materials in the nature. DFT calculations of IRR at CH_3CH/Fe_2O_3 interface[19] revealed that the I_2 molecule directly dissociate on the top of five-coordinated surface Fe^{3+} ion, and the Fe-I bond will be significantly elongated on the transition state (Fig. 9d-f). This reaction pattern is quite similar

to that of Pt(111) (Fig. 9a-c), and μ_{I*}^{o} of Fe_2O_3(012) and Fe_2O_3(104) were estimated to be 0.51 and 0.42 eV, respectively. To validate our estimation, the standard Gibbs free energy profiles of the whole CE reaction on Pt(111), Fe_2O_3(104), and Fe_2O_3(012) were calculated at U = 0.61V vs SHE (Figure 9g). Both Fe_2O_3(104) and Fe_2O_3(012) show considerably lower energy barriers of reaction (24), which confirms kinetically the high activity of Fe_2O_3(104) and Fe_2O_3(012). Similarly, another transition metal oxide, the RuO_2 nanocrystal (μ_{I*}^{o} = 0.59 eV),[76] was also expected and proved to good CE material of DSSC. In addition to the metal oxides, metal sulfide can also be possible CE material candidates. For example, μ_{I*}^{o} of the (0001) surface of NiS nanosheet was calculated to be 0.62 eV, and it indeed exhibits a light conversion efficiency of 8.62% in DSSC, higher than that of Pt-based DSSCs (7.36%).[75]

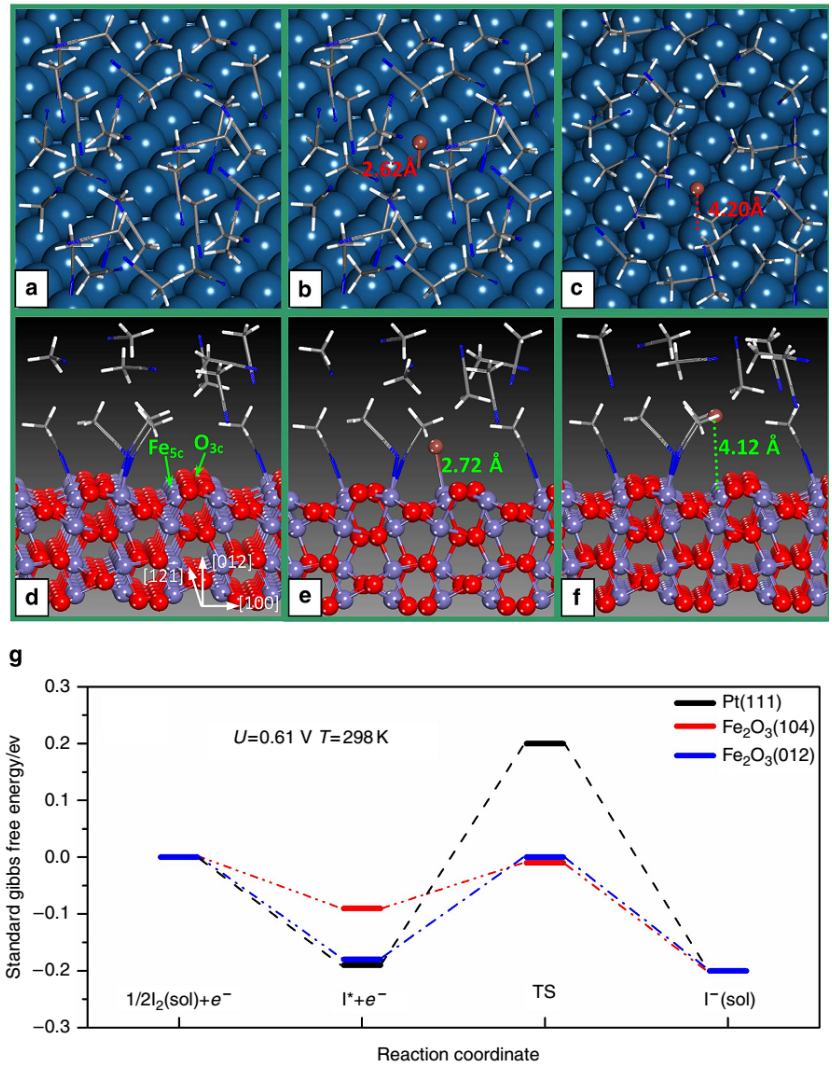

Figure 9. (a-c) Pt(111) surface structure in the presence of CH_3CN solvent, *I* adsorption structure and the transition-state structure. (d–f) For the α-Fe_2O_3(012) surface, similar with a–c. (g) Energy profiles of the whole CE reaction on Pt(111), Fe_2O_3(104) and Fe_2O_3(012), respectively, which were calculated at $U = 0.61$V vs SHE. Reprinted from ref.[19] with permission from Nature Publishing Group.

In addition, under the guidance of activity window for IRR, we successfully modified In_2O_3, initially an inert material for CE in DSSC, into a superior electrocatalyst by doping N heteroatoms. DFT calculations indicated that μ_{I*}^{o} of CH_3CN/N-In_2O_3 (μ_{I*}^{o} = 0.94 eV) is significantly enhanced compared to pure In_2O_3 (μ_{I*}^{o} = 0.16 eV) which is originally outside of the "good IRR catalysts" region.[80] Experiments confirmed that N modified In_2O_3 do hold much

higher IRR activity than its N-free counterpart.

Overall, our method showed quite successful applications on screening the CE materials of DSSC. For a simple reaction like IRR, the reaction mechanism is the same among different catalysts, and there is only one key intermediate (I*). However, when the reaction network becomes complicated there would be many intermediates and the key intermediate could be changed on different catalysts. To address this problem, a careful investigation of the chemistry and mechanism of the reaction should be firstly carried out. Many complicate reactions could be simplified into more affordable ones,[59] and a small-scale test would be conducted before large-scale screening to ensure the reliability of the descriptor. Also, an increasing number of studies now are employing more than one intermediates as the descriptors to evaluate the catalysts.[7, 69]

Concluding remarks and future challenges

In this paper, we reviewed important concepts and understandings on the rational design of heterogeneous catalysts by quantum-chemical calculations. Some general trends and relationships, such as BEP relation and the volcano curve, were covered, which serve as cornerstones for many state-of-the-art designing techniques. Specifically, the theory of the kinetics of chemical potentials in heterogeneous was introduced in detail with mathematical derivations. The applications of this catalyst screening method on designing efficient CE materials for DSSC were reviewed with experimental confirmation.

Currently, although we can obtain the optimal adsorption energy for the key intermediate by identifying the BEP relation and solving micro-kinetics as shown in Figure 7, it requires a

certain amount of DFT calculations, and the micro-kinetics of the systems is sometimes very hard to solve. To primarily estimate this value, we are developing a simple and effective method to estimate the optimal adsorption energy in heterogeneous catalysis. In addition, we are to improve the theoretic framework of multi-phase catalysis,[32, 38] which may break the limitation of the volcano curve and show better activity than tradition catalysts. Coverage effects[87, 88] are also worth taking into account in the rational design of catalysts in the future.

Acknowledges

This project was supported by the National Key Basic Research Program of China (2013CB933201), the National Natural Science Foundation of China (21303052, 21333003, 21622305), Shanghai Rising-Star Program (14QA1401100), "Chen Guang" project (13CG24), Young Elite Scientist Sponsorship Program by CAST, Fundamental Research Funds for the Central Universities, and Special Program for Applied Research on Super Computation of the NSFC-Guangdong Joint Fund (the second phase). Y.M. thanks the Queen's University of Belfast and Chinese Scholarship Council for a joint scholarship.

References

1. Ertl G, Knözinger H, Schuth F, Weitkamp J. *Handbook of Heterogeneous Catalysis, 2nd Edition*. Weinheim: Wiley–VCH; 2008.
2. Robert S. Heterogeneous Catalysis. *Angew Chem Int Ed* 2015, 54:3465-3520.
3. Gerhard E. Reactions at Surfaces: From Atoms to Complexity (Nobel Lecture). *Angew Chem Int Ed* 2008, 47:3524-3535.
4. Zaera F. New Challenges in Heterogeneous Catalysis for the 21st Century. *Catal Lett* 2012, 142:501-516.
5. Wang HF, Kavanagh R, Guo YL, Guo Y, Lu GZ, Hu P. Structural origin: Water deactivates metal oxides to CO oxidation and promotes low-temperature CO oxidation with metals. *Angew Chem Int Ed* 2012, 51:6657-6661.
6. Wang HF, Kavanagh R, Guo YL, Guo Y, Lu G, Hu P. Origin of extraordinarily high catalytic activity of Co3O4 and its morphological chemistry for CO oxidation at low temperature. *J Catal* 2012, 296:110-119.
7. Falsig H, Hvolbæk B, Kristensen IS, Jiang T, Bligaard T, Christensen CH, Nørskov JK. Trends in the catalytic CO oxidation activity of nanoparticles. *Angew Chem Int Ed* 2008, 47:4835-4839.
8. Zhang J, Zhong Z, Cao XM, Hu P, Sullivan MB, Chen L. Ethanol steam reforming on rh catalysts: Theoretical and experimental understanding. *ACS Catal* 2014, 4:448-456.
9. Jones G, Jakobsen JG, Shim SS, Kleis J, Andersson MP, Rossmeisl J, Abild-Pedersen F, Bligaard T, Helveg S,

Hinnemann B, et al. First principles calculations and experimental insight into methane steam reforming over transition metal catalysts. *J Catal* 2008, 259:147-160.

10. Besenbacher F, Chorkendorff I, Clausen BS, Hammer B, Molenbroek AM, Nørskov JK, Stensgaard I. Design of a Surface Alloy Catalyst for Steam Reforming. *Science* 1998, 279:1913-1915.
11. Mao Y, Wang Z, Wang H-F, Hu P. Understanding Catalytic Reactions over Zeolites: A Density Functional Theory Study of Selective Catalytic Reduction of NOx by NH3 over Cu-SAPO-34. *ACS Catal* 2016:7882-7891.
12. Mao Y, Wang H-F, Hu P. Theoretical investigation of NH3-SCR processes over zeolites: A review. *Int J Quantum Chem* 2015, 115:618-630.
13. Janssens TVW, Falsig H, Lundegaard LF, Vennestrøm PNR, Rasmussen SB, Moses P, Giordanino F, Borfecchia E, Lomachenko KA, Lamberti C, et al. A Consistent Reaction Scheme for the Selective Catalytic Reduction of Nitrogen Oxides with Ammonia. *ACS Catal* 2015, 5:2832-2845.
14. Medford AJ, Wellendorff J, Vojvodic A, Studt F, Abild-Pedersen F, Jacobsen KW, Bligaard T, Nørskov JK. Assessing the reliability of calculated catalytic ammonia synthesis rates. *Science* 2014, 345:197-200.
15. Song T, Hu P. Insight into the adsorption competition and the relationship between dissociation and association reactions in ammonia synthesis. *J Chem Phys* 2007, 127:234706.
16. Honkala K, Hellman A, Remediakis IN, Logadottir A, Carlsson A, Dahl S, Christensen CH, Nørskov JK. Ammonia Synthesis from First-Principles Calculations. *Science* 2005, 307:555-558.
17. Wang Z, Hu P. Towards rational catalyst design: a general optimization framework. *Philos Trans A Math Phys Eng* 2016, 374:20150078.
18. Wang Z, Hu P. Some Attempts in the Rational Design of Heterogeneous Catalysts Using Density Functional Theory Calculations. *Top Catal* 2015, 58:633-643.
19. Hou Y, Wang D, Yang XH, Fang WQ, Zhang B, Wang HF, Lu GZ, Hu P, Zhao HJ, Yang HG. Rational screening low-cost counter electrodes for dye-sensitized solar cells. *Nat Commun* 2013, 4:1583.
20. Medford AJ, Vojvodic A, Hummelshøj JS, Voss J, Abild-Pedersen F, Studt F, Bligaard T, Nilsson A, Nørskov JK. From the Sabatier principle to a predictive theory of transition-metal heterogeneous catalysis. *J Catal* 2015, 328:36-42.
21. Wolcott CA, Medford AJ, Studt F, Campbell CT. Degree of rate control approach to computational catalyst screening. *J Catal* 2015, 330:197-207.
22. Norskov JK, Bligaard T, Rossmeisl J, Christensen CH. Towards the computational design of solid catalysts. *Nat Chem* 2009, 1:37-46.
23. Schimka L, Harl J, Stroppa A, Grüneis A, Marsman M, Mittendorfer F, Kresse G. Accurate surface and adsorption energies from many-body perturbation theory. *Nat Mater* 2010, 9:741-744.
24. Nozières P, Pines D. Correlation Energy of a Free Electron Gas. *Phys Rev* 1958, 111:442-454.
25. Mortensen JJ, Kaasbjerg K, Frederiksen SL, Nørskov JK, Sethna JP, Jacobsen KW. Bayesian error estimation in density-functional theory. *Phys Rev Lett* 2005, 95.
26. Wang LP, Titov A, McGibbon R, Liu F, Pande VS, Martinez TJ. Discovering chemistry with an ab initio nanoreactor. *Nat Chem* 2014, 6:1044-1048.
27. Miller SL, Urey HC. Organic compound synthesis on the primitive earth. *Science* 1959, 130:245-251.
28. Luehr N, Ufimtsev IS, Martínez TJ. Dynamic Precision for Electron Repulsion Integral Evaluation on Graphical Processing Units (GPUs). *Journal of Chemical Theory and Computation* 2011, 7:949-954.
29. Ufimtsev IS, Martinez TJ. Quantum Chemistry on Graphical Processing Units. 3. Analytical Energy

Gradients, Geometry Optimization, and First Principles Molecular Dynamics. *Journal of Chemical Theory and Computation* 2009, 5:2619-2628.

30. Medford A, Shi C, Hoffmann M, Lausche A, Fitzgibbon S, Bligaard T, Nørskov J. CatMAP: A Software Package for Descriptor-Based Microkinetic Mapping of Catalytic Trends. *Catal Lett* 2015, 145:794-807.
31. Chorkendorff I, Niemantsve JW. *Concepts of Modern Catalysis and Kinetics*. Weinheim: Wiley-VCH; 2003.
32. Wang Z, Wang H-F, Hu P. Possibility of designing catalysts beyond the traditional volcano curve: a theoretical framework for multi-phase surfaces. *Chem Sci* 2015, 6:5703-5711.
33. Bligaard T, Nørskov JK, Dahl S, Matthiesen J, Christensen CH, Sehested J. The Brønsted-Evans-Polanyi relation and the volcano curve in heterogeneous catalysis. *J Catal* 2004, 224:206-217.
34. Becke AD. Perspective: Fifty years of density-functional theory in chemical physics. *J Chem Phys* 2014, 140:18A301.
35. Kohn W, Sham LJ. Self-Consistent Equations Including Exchange and Correlation Effects. *Phys Rev* 1965, 140:A1133-A1138.
36. Hohenberg P, Kohn W. Inhomogeneous Electron Gas. *Phys Rev* 1964, 136:B864-B871.
37. Chen J-F, Mao Y, Wang H-F, Hu P. Reversibility Iteration Method to Understand Reaction Networks and to Solve Micro-Kinetics in Heterogeneous Catalysis. *ACS Catal* 2016, 6:7078-7087.
38. Andersen M, Medford AJ, Nørskov JK, Reuter K. Analyzing the Case for Bifunctional Catalysis. *Angew Chem Int Ed* 2016:DOI: 10.1002/anie.201601049.
39. Dumesic JA. *The microkinetics of heterogeneous catalysis*. Washington, DC: American Chemical Society; 1993.
40. Jacob T, Goddard WA. Water formation on Pt and Pt-based alloys: a theoretical description of a catalytic reaction. *Chemphyschem* 2006, 7:992-1005.
41. Michaelides A, Hu P. Density functional theory study of hydroxyl and the intermediate in the water formation reaction on Pt. *J Chem Phys* 2001, 114:513-519.
42. Michaelides A, Hu P. Catalytic water formation on platinum: A first-principles study. *J Am Chem Soc* 2001, 123:4235-4242.
43. Balandin AA. Modern State of the Multiplet Theor of Heterogeneous Catalysis1. In: D.D. Eley HP, Paul BW, eds. *Advances in Catalysis*. Vol. Volume 19: Academic Press; 1969, 1-210.
44. Sabatier P. Hydrogénations et déshydrogénations par catalyse. *Berichte der deutschen chemischen Gesellschaft* 1911, 44:1984-2001.
45. Michaelides A, Liu ZP, Zhang CJ, Alavi A, King DA, Hu P. Identification of General Linear Relationships between Activation Energies and Enthalpy Changes for Dissociation Reactions at Surfaces. *J Am Chem Soc* 2003, 125:3704-3705.
46. Nørskov JK, Bligaard T, Logadottir A, Bahn S, Hansen LB, Bollinger M, Bengaard H, Hammer B, Sljivancanin Z, Mavrikakis M, et al. Universality in heterogeneous catalysis. *J Catal* 2002, 209:275-278.
47. Logadottir A, Rod TH, Nørskov JK, Hammer B, Dahl S, Jacobsen CJH. The Brønsted-Evans-Polanyi relation and the volcano plot for ammonia synthesis over transition metal catalysts. *J Catal* 2001, 197:229-231.
48. Liu ZP, Hu P. General trends in CO dissociation on transition metal surfaces. *J Chem Phys* 2001, 114:8244-8247.
49. Fernandez EM, Moses PG, Toftelund A, Hansen HA, Martínez JI, Abild-Pedersen F, Kleis J, Hinnemann B, Rossmeisl J, Bligaard T, et al. Scaling relationships for adsorption energies on transition metal oxide, sulfide, and nitride surfaces. *Angew Chem Int Ed* 2008, 47:4683-4686.

50. Abild-Pedersen F, Greeley J, Studt F, Rossmeisl J, Munter TR, Moses PG, Skúlason E, Bligaard T, Nørskov JK. Scaling Properties of Adsorption Energies for Hydrogen-Containing Molecules on Transition-Metal Surfaces. *Phys Rev Lett* 2007, 99:016105.
51. Wang S, Temel B, Shen J, Jones G, Grabow LC, Studt F, Bligaard T, Abild-Pedersen F, Christensen CH, Nørskov JK. Universal Brønsted-Evans-Polanyi relations for C-C, C-O, C-N, N-O, N-N, and O-O dissociation reactions. *Catal Lett* 2011, 141:370-373.
52. Yang B, Burch R, Hardacre C, Headdock G, Hu P. Understanding the Optimal Adsorption Energies for Catalyst Screening in Heterogeneous Catalysis. *ACS Catal* 2014, 4:182-186.
53. Montemore MM, Medlin JW. Scaling relations between adsorption energies for computational screening and design of catalysts. *Catal Sci Tech* 2014, 4:3748-3761.
54. Mao Y, Chen JF, Wang H-F, Hu P. Catalyst Screening: Refinement of the Origin of the Volcano Curve and its Implication in Heterogeneous Catalysis. *Chin J Catal* 2015, 36:1596-1605.
55. Bligaard T, Nørskov JK, Dahl S, Matthiesen J, Christensen CH, Sehested J. The Brønsted–Evans–Polanyi relation and the volcano curve in heterogeneous catalysis. *Journal of Catalysis* 2004, 224:206-217.
56. Norskov JK, Abild-Pedersen F, Studt F, Bligaard T. Density functional theory in surface chemistry and catalysis. *Proc Natl Acad Sci U S A* 2011, 108:937-943.
57. Studt F, Abild-Pedersen F, Bligaard T, Sørensen RZ, Christensen CH, Nørskov JK. Identification of non-precious metal alloy catalysts for selective hydrogenation of acetylene. *Science* 2008, 320:1320-1322.
58. Vojvodic A, Nørskov JK. New design paradigm for heterogeneous catalysts. *National Science Review* 2015, 2:140-143.
59. Studt F, Sharafutdinov I, Abild-Pedersen F, Elkjær CF, Hummelshøj JS, Dahl S, Chorkendorff I, Nørskov JK. Discovery of a Ni-Ga catalyst for carbon dioxide reduction to methanol. *Nat Chem* 2014, 6:320-324.
60. Stegelmann C, Andreasen A, Campbell CT. Degree of rate control: how much the energies of intermediates and transition states control rates. *J Am Chem Soc* 2009, 131:8077-8082.
61. Campbell CT. Finding the Rate-Determining Step in a Mechanism: Comparing DeDonder Relations with the "Degree of Rate Control". *J Catal* 2001, 204:520-524.
62. Calle-Vallejo F, Loffreda D, Koper MTM, Sautet P. Introducing structural sensitivity into adsorption–energy scaling relations by means of coordination numbers. *Nat Chem* 2015, 7:403-410.
63. Calle-Vallejo F, Tymoczko J, Colic V, Vu QH, Pohl MD, Morgenstern K, Loffreda D, Sautet P, Schuhmann W, Bandarenka AS. Finding optimal surface sites on heterogeneous catalysts by counting nearest neighbors. *Science* 2015, 350:185-189.
64. Cheng J, Hu P. Theory of the Kinetics of Chemical Potentials in Heterogeneous Catalysis. *Angew Chem Int Ed* 2011, 50:7650-7654.
65. Hecht CE. *Statistical thermodynamics and kinetic theory*. New York: W. H. Freeman; 1990.
66. Gupta MC. *Statistical thermodynamics*. Chichester: Wiley; 1990.
67. Xing J, Jiang HB, Chen JF, Li YH, Wu L, Yang S, Zheng LR, Wang HF, Hu P, Zhao HJ, et al. Active sites on hydrogen evolution photocatalyst. *J Mater Chem A* 2013, 1:15258-15264.
68. Cheng J, Hu P, Ellis P, French S, Kelly G, Lok CM. Brønsted−Evans−Polanyi Relation of Multistep Reactions and Volcano Curve in Heterogeneous Catalysis. *J Phys Chem C* 2008, 112:1308-1311.
69. Cheng J, Hu P. Utilization of the Three-Dimensional Volcano Surface To Understand the Chemistry of Multiphase Systems in Heterogeneous Catalysis. *J Am Chem Soc* 2008, 130:10868-10869.
70. Stoltze P. Microkinetic simulation of catalytic reactions. *Prog Surf Sci* 2000, 65:65-150.

71. Dumesic JA. Analyses of Reaction Schemes Using De Donder Relations. *J Catal* 1999, 185:496-505.
72. O'Regan B, Gratzel M. A low-cost, high-efficiency solar cell based on dye-sensitized colloidal TiO2 films. *Nature* 1991, 353:737-740.
73. Tang Q, Cai H, Yuan S, Wang X. Counter electrodes from double-layered polyaniline nanostructures for dye-sensitized solar cell applications. *J Mater Chem A* 2013, 1:317-323.
74. Lee KS, Lee HK, Wang DH, Park N-G, Lee JY, Park OO, Park JH. Dye-sensitized solar cells with Pt- and TCO-free counter electrodes. *Chem Comm* 2010, 46:4505-4507.
75. Li Y, Wang H, Zhang H, Liu P, Wang Y, Fang W, Yang H, Li Y, Zhao H. A {0001} faceted single crystal NiS nanosheet electrocatalyst for dye-sensitised solar cells: sulfur-vacancy induced electrocatalytic activity. *Chem Comm* 2014, 50:5569-5571.
76. Hou Y, Chen ZP, Wang D, Zhang B, Yang S, Wang HF, Hu P, Zhao HJ, Yang HG. Highly electrocatalytic activity of ruo2 nanocrystals for triiodide reduction in dye-sensitized solar cells. *Small* 2014, 10:484-492.
77. Lodermeyer F, Costa RD, Casillas R, Kohler FTU, Wasserscheid P, Prato M, Guldi DM. Carbon nanohorn-based electrolyte for dye-sensitized solar cells. *Energy Environ Sci* 2015, 8:241-246.
78. Chen J-F, Mao Y, Wang H-F, Hu P. Theoretical study of heteroatom doping in tuning the catalytic activity of graphene for triiodide reduction. *ACS Catal* 2016, 6:6804-6813.
79. Zhang B, Wang D, Hou Y, Yang S, Yang XH, Zhong JH, Liu J, Wang HF, Hu P, Zhao HJ, et al. Facet-dependent catalytic activity of platinum nanocrystals for triiodide reduction in dye-sensitized solar cells. *Sci Rep* 2013, 3:1836.
80. Zhang B, Zhang NN, Chen JF, Hou Y, Yang S, Guo JW, Yang XH, Zhong JH, Wang HF, Hu P, et al. Turning Indium Oxide into a Superior Electrocatalyst: Deterministic Heteroatoms. *Sci Rep* 2013, 3:3109.
81. Wang L, Al-Mamun M, Liu P, Wang Y, Yang HG, Wang HF, Zhao H. The search for efficient electrocatalysts as counter electrode materials for dye-sensitized solar cells: mechanistic study, material screening and experimental validation. *NPG Asia Mater* 2015, 7:e226.
82. Hagfeldt A, Boschloo G, Sun L, Kloo L, Pettersson H. Dye-Sensitized Solar Cells. *Chem Rev* 2010, 110:6595-6663.
83. Grätzel M. Dye-sensitized solar cells. *J Photochem Photobiol C* 2003, 4:145-153.
84. Lambert C, Mao Y, Zheng Y-Z, Tao X, Hu P, Huang M. Characterization of High-Performance Organic Dyes for Dye-Sensitized Solar Cell: A DFT/TDDFT Study. *Canadian Journal of Chemistry* 2016.
85. Hauch A, Georg A. Diffusion in the electrolyte and charge-transfer reaction at the platinum electrode in dye-sensitized solar cells. *Electrochim Acta* 2001, 46:3457-3466.
86. Wang D, Jiang J, Wang HF, Hu P. Revealing the Volcano-Shaped Activity Trend of Triiodide Reduction Reaction: A DFT Study Coupled with Microkinetic Analysis. *ACS Catal* 2016, 6:733-741.
87. Wang H, Guo Y, Lu G, Hu P. An understanding and implications of the coverage of surface free sites in heterogeneous catalysis. *J Chem Phys* 2009, 130:224701.
88. Lausche AC, Medford AJ, Khan TS, Xu Y, Bligaard T, Abild-Pedersen F, Nørskov JK, Studt F. On the effect of coverage-dependent adsorbate-adsorbate interactions for CO methanation on transition metal surfaces. *J Catal* 2013, 307:275-282.